A COUPLED MULTIPHYSICS ANALYSIS FOR A HYPERSONIC VEHICLE. E. L. Blades[1], E. A. Luke[2], R. S. Miskovish[3] and P. Shah[4], [1]ATA Engineering, Inc. eric.blades@ata-e.com, [2]Center for Advanced Vehicular Systems, Mississippi State University, luke@cse.msstate.edu, [3]ATA Engineering, Inc., scott.miskovish@ata-e.com, [4]ATA Engineering, Inc, parthiv.shah@ata-e.com.

Introduction: The United States Air Force has identified multiphysics coupled analysis capability as an enabling technology to the design of future high-speed vehicles that must withstand extreme aero-thermal and aeroacoustic environments. The expected benefit of such a tool is a more accurate response prediction of the aerothermoelastic phenomena of panel hot spots, snap-through, and/or flutter, to enable designs that do not carry a weight penalty due to over-specification of thermal protection systems.

The design of such combined environment structures requires a time-resolved definition of the vehicle's aero-thermal environments along a given trajectory and mission. The vehicle's thermal-vibro-acoustic behavior must be coupled to a mission profile. High temperatures along the trajectory require unconventional lightweight materials to be used for vehicle skin panels, such as fiber-reinforced composites, metal matrix composites, and intermetallic compounds [1]. As the vehicle accelerates, aerodynamic heating takes place on the panels due to several phenomena. In the supersonic region, the bow shock continuously deforms along the trajectory, with large temperature and pressure gradients across it. The increasing kinetic energy of the flow heats the panel, deforming it into the flow and further inducing spatial temperature gradients that can feed back on local deformations, causing dangerous "hot spots." Panel deformations can also induce local shocks due to effective curvature changes, resulting in shock-boundary layer interactions (SBLI) and strong aerothermoelastic coupling, which may result in dangerous panel flutter or snap-through responses. Additional loading scenarios on vehicle skin panels include local flow separation, strong shocks, and shock impingement on downstream control surfaces.

This paper presents selected results generated in ATA Engineering, Inc.'s (ATA) Phase I Air Force Research Laboratory (AFRL)-sponsored SBIR program for the "Development of a Multiphysics, Coupled Analysis Framework for Hypersonic Vehicle Structures." The long-term goal of the SBIR program is to develop a physics simulation capability that encompasses a set of coupled software tools that could be used for vehicles exposed to launch, flight in air at sustained hypersonic velocities, and re-entry, and for stealth aircraft with buried engines and ducted exhaust.

A notional hypersonic vehicle forebody is shown in Figure 1(a). The vehicle underbody ramps are compression surfaces of 3, 7, and 11 degrees, respectively. The forebody was similar to the vehicle described in Blevins et al. [2] with a typical mission profile to Mach 15 at constant dynamic pressure of 1000 lb/ft^2. This is an example of a candidate hypersonic cruise mission envelope for a blended wing body (BWB) aircraft. Typically, such a vehicle design requires more propulsion system/airframe integration than conventional military and commercial aircraft.

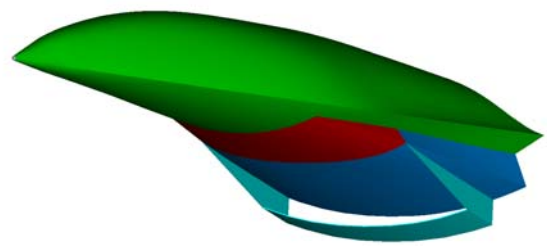

(a)

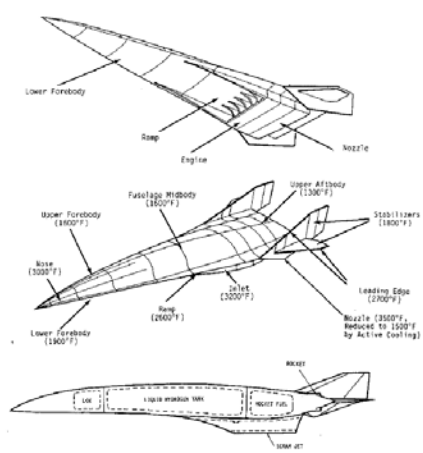

(b)

Figure 1. A candidate hypersonic flight vehicle fore-body (a) based on the vehicle described in Blevins et al. (1993) (b)

In the Mach-altitude plane shown in Figure 2, the ascent portion of a typical trajectory of such a vehicle

may last on the order of fifteen minutes. It is bounded by a minimum stagnation pressure limit for air-breathing combustion and a maximum dynamic pressure limit for structural loading. The ascent portion of the trajectory benefits from high altitude flight due to a lower dynamic pressure trajectory and lower max skin temperatures. Re-entry (descent) lasts on the order of 45 minutes. Here, the air-breathing engines are disabled, and re-entry heating must be minimized. The vehicle aerodynamic and structural design is largely driven by thermal management requirements.

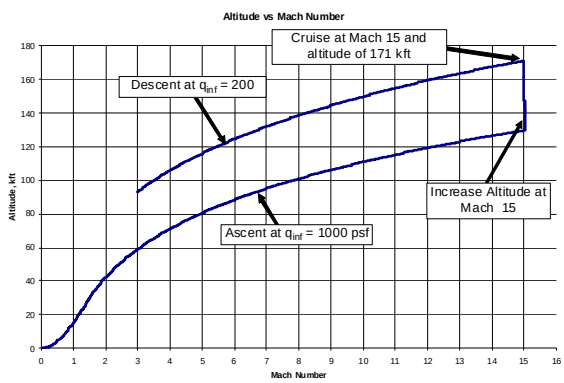

Figure 2. Typical trans-atmospheric flight trajectories for a candidate hypersonic flight vehicle

Discussion: The objective of this work was to perform an iteratively coupled multiphysics analysis of a representative hypersonic skin panel in a combined, extreme loading environment. The specific coupling referred to here is between the CHEM CFD solver [3] (that includes chemically reacting physics models) working in the Loci framework [4] and the nonlinear computational structural dynamics (NLCSD) solver Abaqus. The term "iteratively coupled" is used here to imply that solution data between CFD and NLCSD solvers is passed back and forth at each iteration. In this work, the data exchange occurred manually. Efforts are underway to develop the appropriate coupling tools to automate this process in a straight forward manner. The CFD data that is passed includes pressures and temperatures that are applied in the NLCSD, which subsequently passes back a deflected panel shape. The CFD volume grid is manually regenerated to reflect the deflected panel shape.

Uncoupled CFD Simulations. Two- and three-dimensional CFD simulations of the hypersonic vehicle were run at the design Mach number of 15 and altitude of 129,900 ft. The simulations were performed at the Mississippi State University (MSU) Center for Advanced Vehicular Systems (CAVS SimCenter). The CFD simulations employ the five-species, seventeen reaction finite-rate chemistry model for air developed by Kang and Dunn [5] utilizing a vibrational equilibrium model for diatomic species. Laminar transport properties for mixture viscosity, conductivity, and species diffusion are provided using a CHEMKIN property database. Turbulence is modeled using Menter's SST [6] turbulence model employing the Sarkar's compressibility correction [7]. An adaptive Riemann solver based on Quirk's formulation [8] was employed to improve numerical stability in the strong leading bow shock region of the flow. A solution-adaptive mesh refinement strategy was employed using error estimators and techniques described in a recent paper [9].

Two-Dimensional CFD Simulations. The vehicle was modeled using both two- and three-dimensional models of a representative geometry at zero degrees angle of attack. The flow conditions at an altitude of 129,900 ft and a Mach number of 15 were simulated. To simulate this altitude, the free-stream pressure and temperature were set to 293.3 Pascals and 250 Kelvin, respectively.

Contours plots of Mach number, pressure, mass fraction of the nitric oxide (NO) species, and temperature from the two-dimensional simulations are presented in Figure 3 to Figure 6, respectively. Figure 4 also shows an image of the mesh. For the two-dimensional simulations, two levels of solution-adaptive refinement were utilized. The mesh size ranged from 50,000–200,000 cells depending on the case and refinement level. The 200,000-cell grids were likely in excess of the minimum requirements for this type of problem.

Figure 7 and Figure 8 show plots of the underside pressure distribution and heat flux as a function of streamwise distance along the vehicle. Two CFD cases are shown, one with the nominal vehicle (black) and another with a local deflection introduced on the 12-inch ramp panel located approximately 55 feet aft of the nose (blue). The local panel was deformed according to a cosine profile, with point and slope continuity on either end. The total amount of deflection was set to one percent of the panel length, as depicted in Figure 61. A new grid was generated for this case which includes an enrichment of points in the deformed region. In general, the two CFD results lie on top of each other except very locally where the panel deflection occurs and in the extreme downstream stations. CFD results also show a reasonable comparison to the quasi-one-dimensional results obtained using MINIVER [10] (shown in red).

For heat flux estimations, a fixed temperature estimated from the MINIVER radiation equilibrium wall

temperature analysis in the ramp region was used for the vehicle surface temperatures. The present model considered an inert wall that did not participate in the chemical reactions through catalytic mechanisms. Thus the heat fluxes presented here are underpredicted. Figure 10 shows a zoomed-in view of the predicted heat flux. From the figure, it becomes clear that a one-percent panel deflection results in a ± 8 % change in the local heat flux. Based on the local flowfield, a one-percent panel deflection is estimated to be 1, 8, and 4 percent of the displacement, momentum, and energy thicknesses, respectively, as defined by Schlicting and Gersten [11]. This suggests that a local hot spot can be easily generated in this region from a relatively small deflection. When this is compared to the nearly four-percent deflection seen in the transient thermal-structural study [12], which is discussed in the next section, the two-dimensional simulations suggest that large increases in heat flux of twenty or thirty percent may be achievable from local deformation.

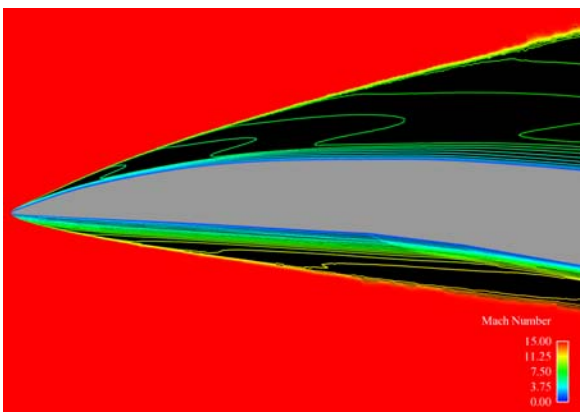

Figure 3. Mach number contours

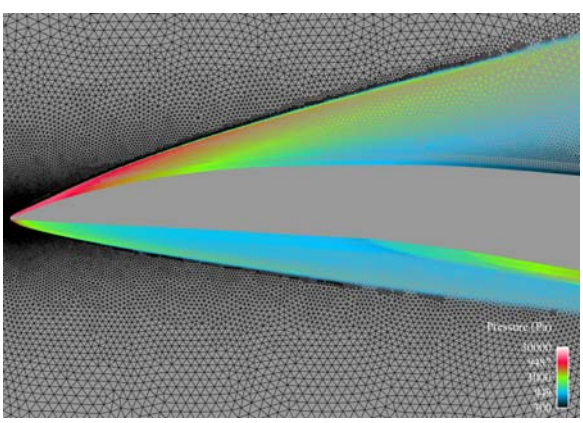

Figure 4. Pressure contours and mesh density plot

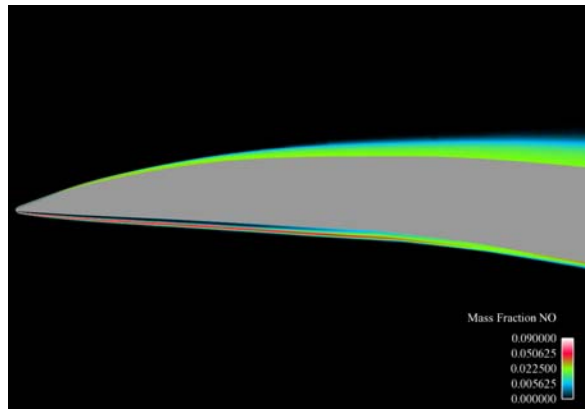

Figure 5. Mass fraction of NO species

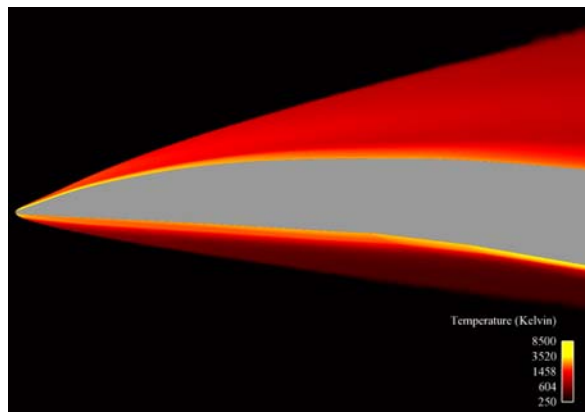

Figure 6. Temperature distribution

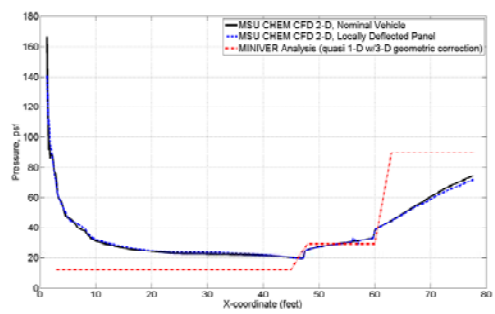

Figure 7. Pressure along vehicle underside

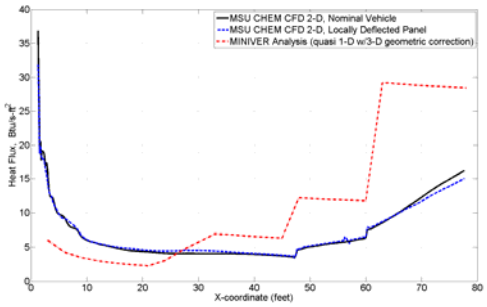

Figure 8. Underbody heat flux

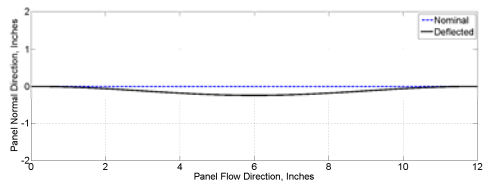

Figure 9. Modeled ramp panel deflection of one percent of total length based on cosine shape function

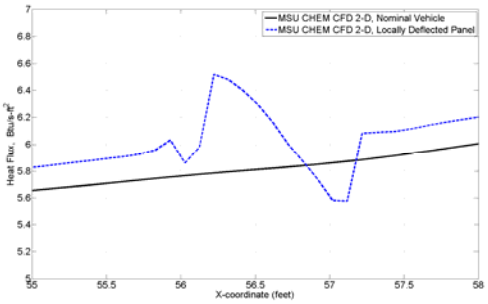

Figure 10. Zoomed-in view of heat flux at deflected panel location showing ± 8 percent heat flux variation at location of 1 percent panel deflection

Three-Dimensional CFD Simulations. Initially, 3-D CFD computations were conducted for the vehicle forebody depicted in Figure 1 at zero degrees AoA. Under this condition, it was found that the vehicle was not a lifting body. Additionally, it was found that heat transfer was reduced along the symmetry line of the bottom of the vehicle due to an effect of flow spilling over the edge of the vehicle from top to bottom. By running simulations at 2, 4, and 6 degrees angle of attack, it was found that 6 degrees AoA resulted in a positive lift. In addition, the heat transfer along the bottom of the vehicle no longer presented a reduction along the line of symmetry. Therefore, results at six degrees AoA are presented here, with a freestream Mach number of 15 and at an altitude of 129,900 feet. The same solver parameters were used for the 3-D as were used for the 2-D simulations.

After performing a smooth vehicle simulation, several simulations were performed for vehicles with a locally deformed panel on the 11-degree ramp. To reduce the size of the problem, symmetry was utilized for both the smooth and deformed vehicle panels by generating a half-plane model and applying appropriate boundary conditions along the vehicle centerline. The volume meshes contained approximately 3M points and 10M cells. The CFD simulations took approximately two days and utilized 84 processors, including grid adaptations to adequately define the detached bow shock emanating from the nose of the vehicle.

The panel deformations applied to the CFD simulations were based on a transient thermal structural simulation of a curved panel subjected to fluctuating pressure level (FPL) loadings to simulate phenomena such as snap-through buckling [12]. The Inconel X-750 panel definition was based on communication with Wright-Patterson AFB [13]. The metallic panel length and width are 12 by 18 inches, with a nominal thickness of 0.060 inch. The material properties for Inconel X-750 are based on MIL-HDBK-5J and are presented in Appendix A.

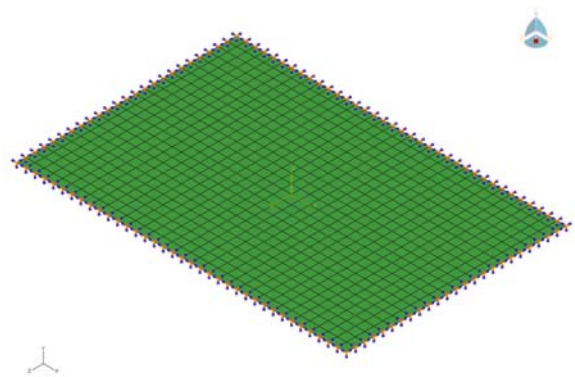

Figure 11. Representative panel FEM with clamped edge constraints

The maximum resulting panel deflection for the Inconel simulation was found to be about 0.6 inches, or 5% of the streamwise length. A panel with this type of deflection was placed in the engine inlet region on the 11-degree ramp, about 66 feet from the nose of the

vehicle. An engine inlet cowl was added to the simulation to create shock-boundary layer interactions which would yield more extreme heating and acoustic loading on the panel.

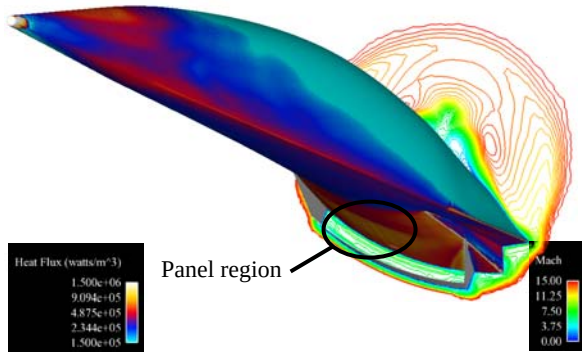

Figure 12. CFD simulation of vehicle forebody plus engine inlet cowl at six degrees AoA. Split image shown with deflected panel to the right of the vehicle symmetry plane. Heat flux values shown on vehicle surfaces, while isocontours of Mach number are shown at a constant axial location near the domain exit

The first simulation placed the panel in the center of the inlet ramp, as shown in Figure 12 and Figure 13. The arrows in Figure 13 and subsequent figures are used for orientation and indicate the direction of the freesteam flow. Simulations predict a significant perturbation in computed heat transfer for the deformed panel showing nearly an order of magnitude difference between the largest and smallest heat flux on the panel. Pressure contours show a similar range of pressure disturbances. The 0.6-inch panel deflection represents about 50, 450, and 250 percent of the displacement, momentum, and energy thickness, respectively, as defined by Schlicting and Gersten [11]. This clearly puts this level of deflection in a different regime when compared to the two-dimensional panel deflected by one percent of its streamwise length that was discussed in the previous subsection. For the current 3-D simulation, the large deflection can be conjectured to introduce a large perturbation to the flowfield, resulting in much larger heat transfer perturbations.

A subsequent simulation placed the panel next to the inlet sidewall where strong shocks form. As shown in Figure 14 and Figure 15, there is significant interaction between the shock and boundary layers. The overall heat transfer for the vehicle is shown in Figure 14. A zoomed-in image on the right side of Figure 15 shows the detail of the heat flux. Pressure contours are also plotted along a cutting plane just ahead of the panel. The pressure contours clearly show a lambda shock structure caused by the shock formed on the inlet sidewall interacting with the boundary layer that exists along the body of the vehicle. As a result of the lambda shock structure, two shocks impinge on the surface of the inlet ramp. The panel was positioned such that both shocks intersect the panel. Again, significant changes in the surface heat transfer occur due to the panel deformation. In fact, heat transfer in this location can be similar to the nose heating. Pressure contours are shown on the left side of Figure 15. The locations of the shocks impinging on the panel are clearly visible.

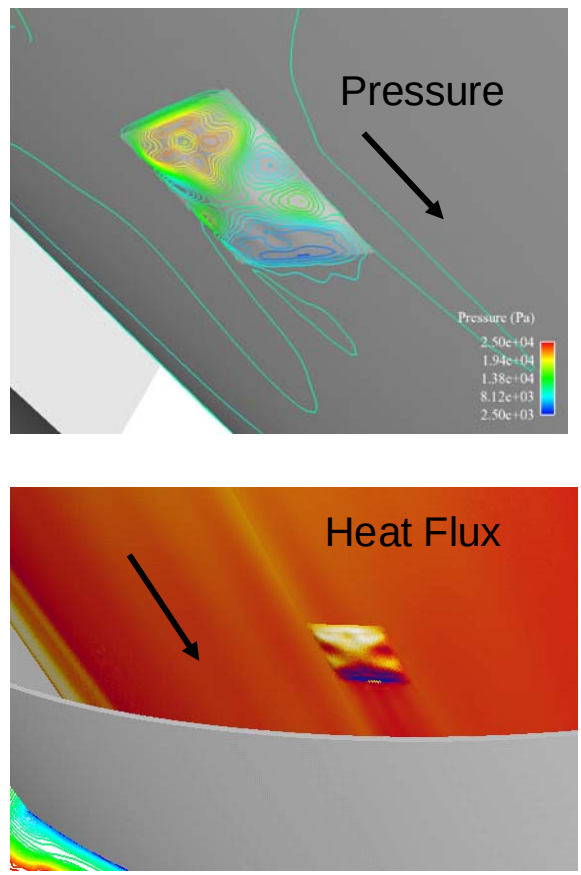

Figure 13. Pressure isocontours (left) and heat flux contours (right) for vehicle underbody with deflected panel along vehicle centerline. Black arrow indicates primary airflow direction

It is worth noting that the panel in this location experiences a pressure variation of two orders of magnitude. For SBLI on a two-dimensional compression ramp, fluctuating pressure level is often estimated using an empirically derived formula such as those given

by Laganelli [14]. To estimate the rise in acoustic level on the structure, the following expression is used to estimate the peak pressure rise at a compression corner:

$$\left(\frac{p_{rms}}{q_\infty}\right) \cong \left(\frac{p_{rms}}{q_\infty}\right)_{\mathrm{TBL}} \left[A + B\left(\frac{P_{w_2}}{P_{w_1}}\frac{2.95}{M_1}\right)_{\max,\phi} + C\left(\frac{P_{w_2}}{P_{w_1}}\frac{2.95}{M_1}\right)^2_{\max,\phi} \right]$$

where A = -1.181, B = 1.713, and C = 0.468. It is clear that the pressure rise across such shocks, P_{w_2}/P_{w_1}, is the driving term in this equation. It is therefore plausible to suggest that these strong SBLI flowfields may be suitable environments to generate the type of snap-through/buckling of vehicle panels that have been previously discussed.

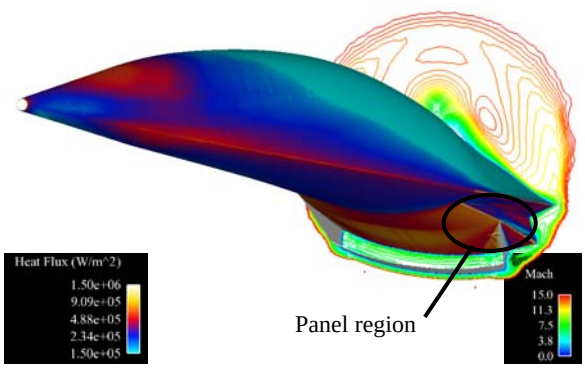

Figure 14. CFD simulation of vehicle forebody plus engine inlet cowl at six degrees AoA. Deflected panel located on vehicle underside near engine inlet sidewall (indicated by arrow). Heat flux values shown on vehicle surfaces. Isocontours of Mach number are shown at a constant axial location near the domain exit

As a final comment on the design of hypersonic vehicles, it should be noted that the current vehicle and inlet definition has be generated using crude approximations. For example, a realistic inlet design would consider the vehicle flowfields at several operating flight Mach numbers and attempt to optimize the geometry to minimize losses that may occur from aerodynamic shocks. No such design exercise has been undertaken here, and thus the strength of SBLI may be somewhat exaggerated for illustrative purposes. Future efforts will be based on a more realistic vehicle.

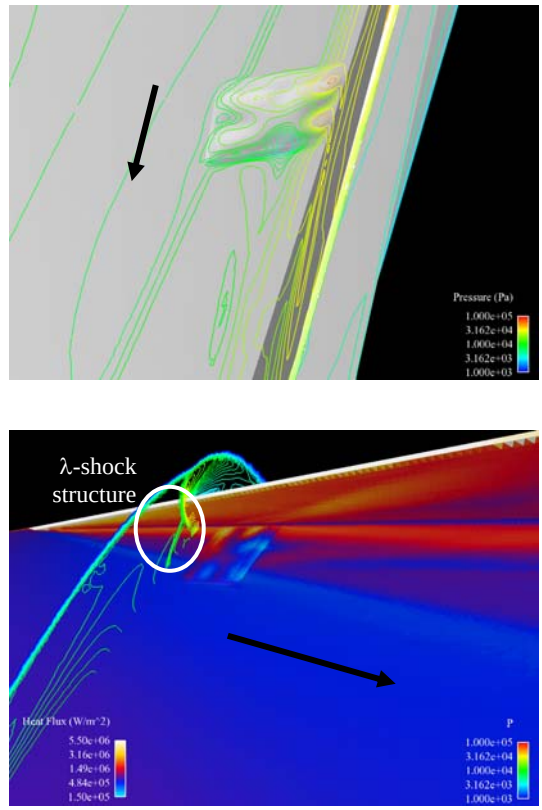

Figure 15. Pressure isocontours (left) and heat flux contours (right) for vehicle underbody with deflected panel on vehicle underside near engine inlet sidewall. Black arrow indicates primary airflow direction

Iteratively Coupled Quasi-static CFD/NLCSD: The quasi-static deformed panel analysis of Reference [12] was iteratively coupled with the CFD analyses of the previous section to demonstrate that a quasi-static aerothermoelastic equilibrium problem can be solved at the whole vehicle level as a first step in improved accuracy from coupled simulations. For this work, each iteration was a manual process between the CFD analyst and the structural analyst. Efforts are underway to develop an automated process to achieve the final quasi-static vehicle deformed shape and flowfield.

The schematic diagram in Figure 16 describes the process that was employed. In this exercise, the bounding analysis described in Reference [12] was considered for the flat Inconel X-750 panel. At the same time, the 3-D CFD analysis for the vehicle forebody described in the previous section was also performed for the deformed Inconel X-750 (that was nominally flat). The deformations from the panel analysis were applied to the CFD model, changing the local geome-

try of the vehicle. After this update, the CFD simulation was performed, and changes in pressure and temperature were computed. These pressure and temperature changes were then applied to the panel model as additional boundary conditions. The bounding analysis was performed using these updated boundary conditions, and the updated displacements were computed again. For this project, three iterations were performed: one baseline and two revisions.

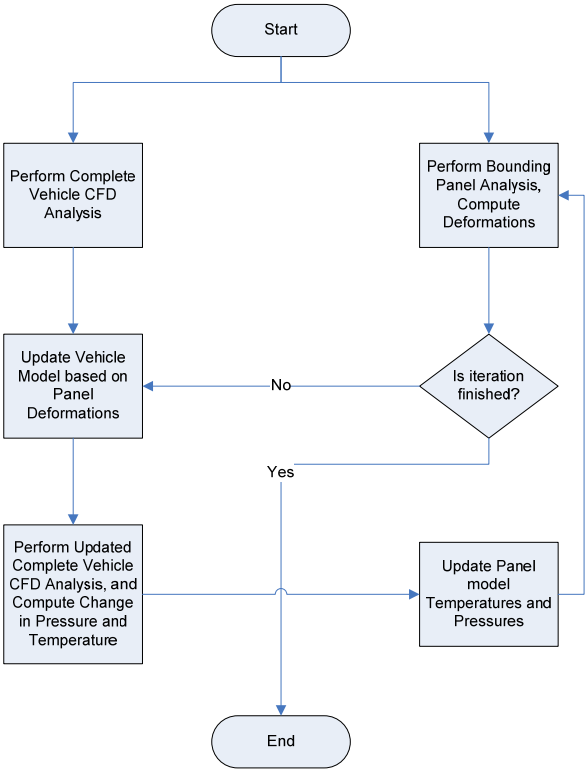

Figure 16. Process to perform iteratively coupled CFD/NLCSD simulation

Figures 17 to 24 show contours of the deflection, pressure, and time on the panel surface at the first three iterations. Note that there was no pressure delta applied to the baseline panel model.

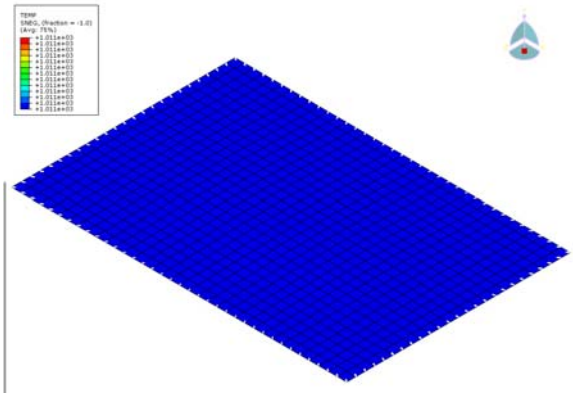

Figure 17. Baseline temperature applied to the panel structural model

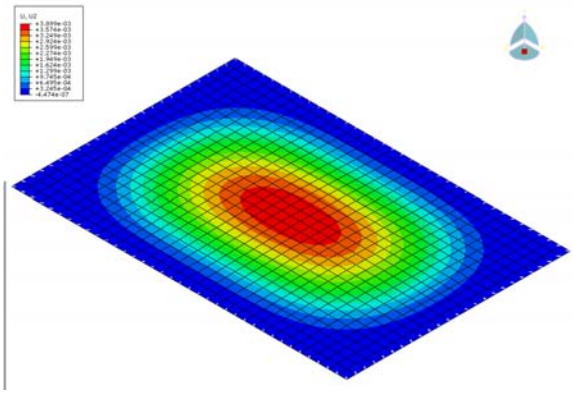

Figure 18. Baseline normal displacements computed for the panel structural model

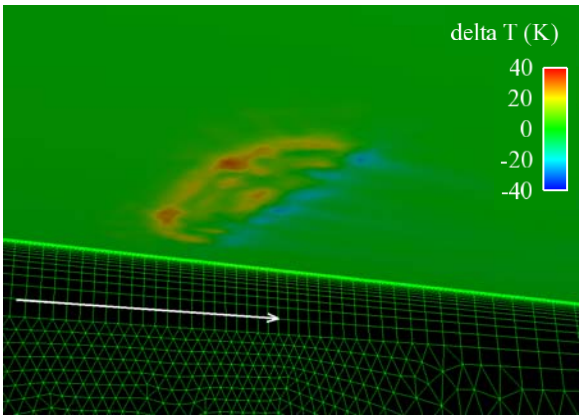

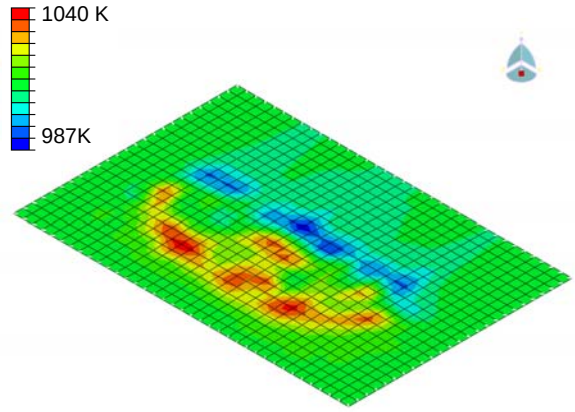

Figure 19. Iteration 1 temperature changes from CFD (top) applied as temperature boundary conditions to the panel structural model (bottom)

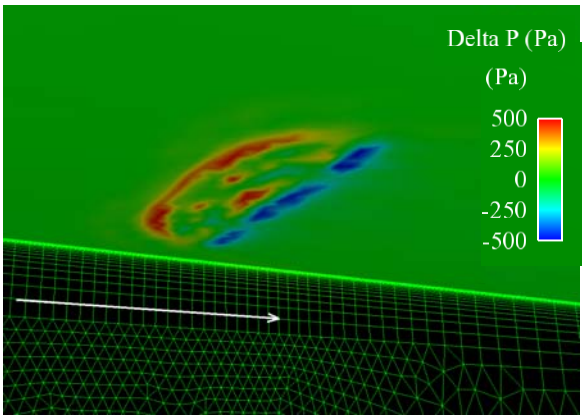

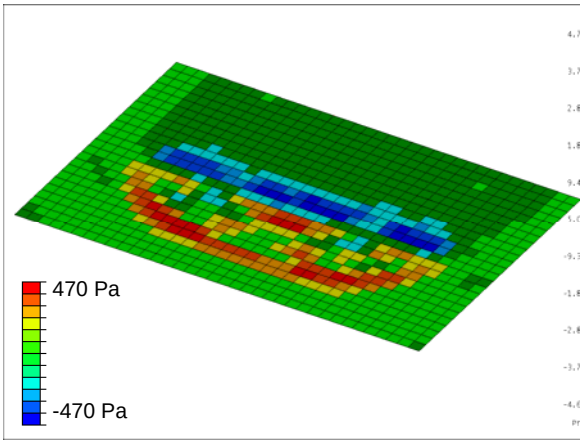

Figure 20. Iteration 1 pressure changes from CFD (top) applied as pressure boundary conditions to the panel structural model (bottom)

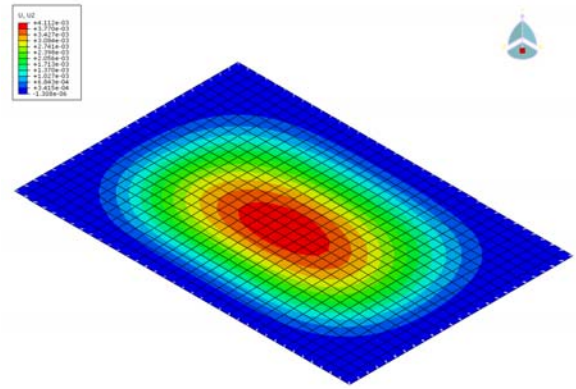

Figure 21. Iteration 1 normal displacements computed for the panel structural model

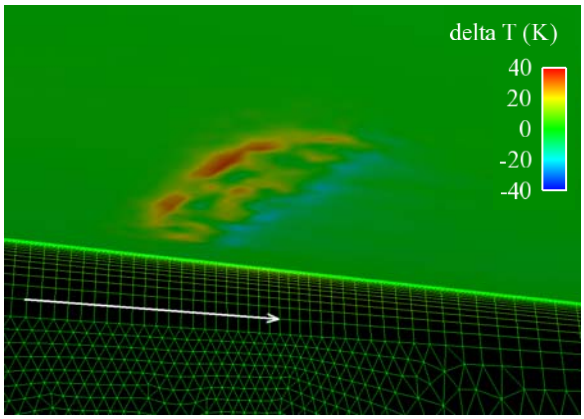

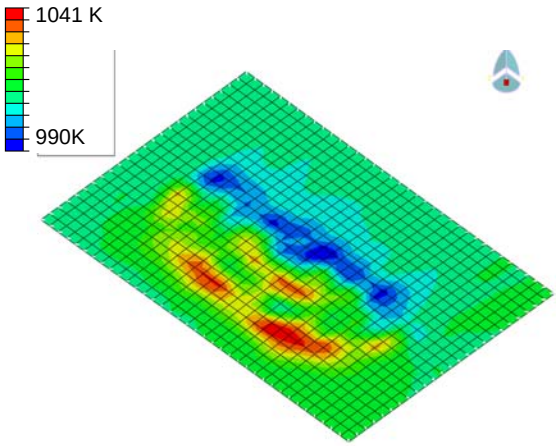

Figure 22. Iteration 2 temperature changes from CFD (top) applied as temperature boundary conditions to the panel structural model (bottom)

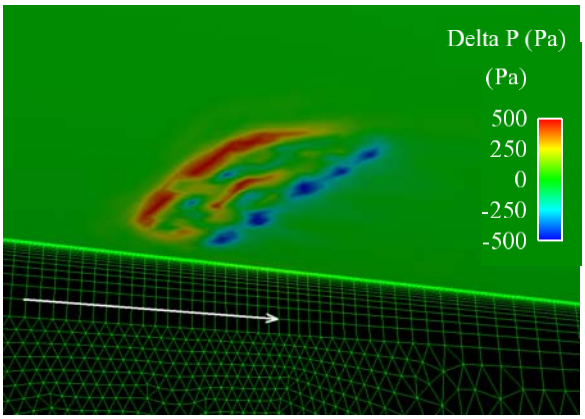

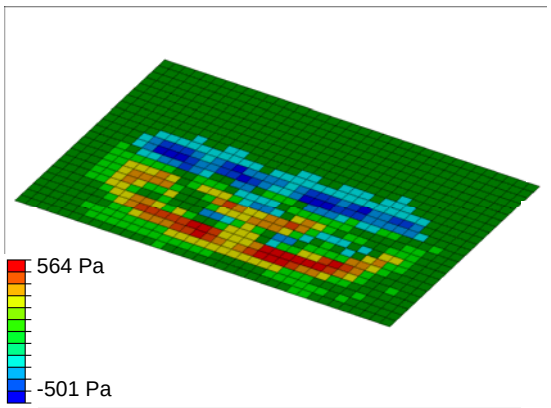

Figure 23. Iteration 2 pressure changes from CFD (top) applied as pressure boundary conditions to the panel structural model (bottom)

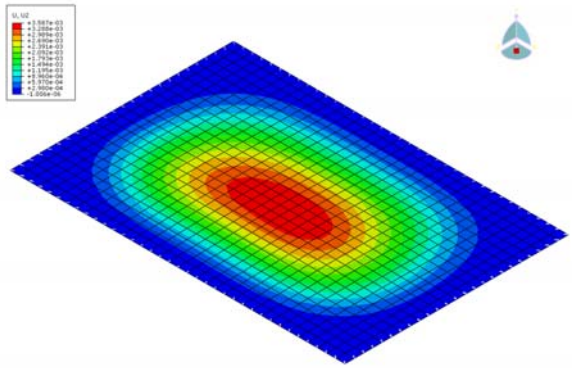

Figure 24. Iteration 2 normal displacements computed for the panel structural model

Looking at the displacement results, the RMS difference between the baseline and Revision 1 was 5.6% of the peak displacement, and 3.4% between Revisions 1 and 2. If the RMS difference decays exponentially, it will take six iterations to go below 1% and ten to go below 0.1% RMS difference. However, there is some oscillation in the pressure, temperature, and peak displacements between iterations, which suggests that an automated method may require iteration damping to aid in the convergence of the panel and vehicle models. Iteration damping would use a linear combination of the old and new results as the inputs into the new solution sequence, and would be controlled by a damping parameter, i.e., $R_{applied} = (1-\alpha)R_{old} + \alpha R_{new}$, where α is the damping parameter $0 \le \alpha \le 1$, $R_{applied}$ is the applied result, R_{old} is the old result, and R_{new} is the new estimate of the result. In the next phase of this research, convergence studies using the relaxation method proposed above will be tested on 2-D geometries for faster turnaround.

To determine the effects of deformed shape on the transient behavior of the panel, a transient pressure load was applied to the three iterations of the deformed Abaqus model. Two 2.138-second transient simulations using 148 and 150 dB FPL values were performed using an integration time step of 1 microsecond. The time history of the displacement at the center node was plotted to determine if the panel exhibits snap-through behavior. The results, shown in Figure 25 and Figure 26, show that there is more snap-through behavior for the revised panel shape over the baseline shape at 148 dB, and that the behavior at 150 dB is similar for all shapes. Therefore, this suggests the change in shape may affect the snap-through behavior at the lower bound of the FPL values, and may trigger snap-through at lower FPL values than were recently investigated.

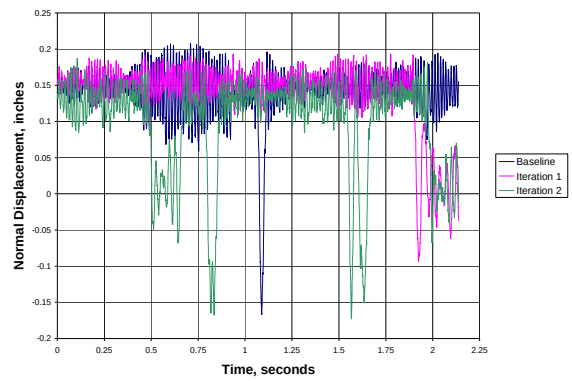

Figure 25. Response of center of a flat plate due to a 148 dB acoustic excitation for three iterations. Displacement is in inches

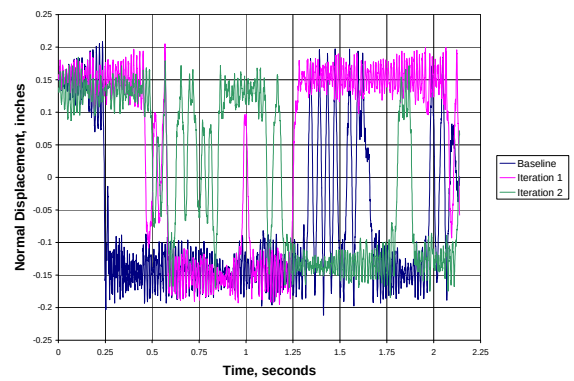

Figure 26. Response of center of a flat plate due to a 150 dB acoustic excitation for three iterations. Displacement is in inches

Summary and Concluding Remarks: The objectives of this work were to characterize regions on a representative hypersonic vehicle where multiphysics coupling is required to accurately predict the skin panel structural response, as well as to develop a computational framework for a multiphysics capability. The multiphysics analysis was conducted using the Loci/CHEM CFD code and the Abaqus/Explicit nonlinear computational structural dynamics code. CFD simulations reveal that small deformations (several percent of panel streamwise length) can lead to relatively large increases in the local heat transfer coefficient that grow nonlinearly with increasing deflection (from tens of percent to several times the local rates). Quasi-static deformations of the skin panels can be significant under the applied aero-thermal loads.

Deflections of up to five percent of the panel streamwise length, or several times the panel thick-

ness, are predicted. In a separate study, it was found that these thermal deformation of a semi-infinite panel may reduce the flutter onset boundary due to curvature effects using methods based on the work of Librescu [15].

Efforts are currently underway to develop a multiphysics computational framework using a two-stage analysis approach, starting with a quasi-static aero-thermal-elastic analysis of the whole vehicle and then progressing to high-fidelity, unsteady aero-thermal-elastic analysis at the local panel level. This framework will couple the Loci/CHEM CFD solver to the Abaqus/Explicit NLCSD solver using SIMULIA's Co-Simulation Engine (CSE). The CSE synchronizes the computational codes at each iteration or time step and handles the data transfer between the codes. A linear elasticity-based mesh deformation algorithm is being implemented into CHEM to automatically move the CFD volume mesh to reflect the vehicle structural deformations.

Acknowledgements: This work was completed with SBIR funding from Wright-Patterson AFB, contract FA8650-09-M-3930, Dr. S. Michael Spottswood, Program Manager.

References:

[1] Vaicaitis, R., (1994), *Journal of Aircraft*, 31(1), 10–18.

[2] Blevins, et al., (1993), *Journal of Aircraft*, 30(6), 971–978.

[3] Luke, E, (2007), AIAA Paper 2007-3956.

[4] Luke, E. and T. George, (2005) *Journal of Functional Programming*, 15(3), 477–502.

[5] Kang, S.W., and Dunn, M.G., (1972), AIAA Paper 72-689.

[6] Menter, F.R., (1994), *AIAA Journal*, 32(8), 188–193.

[7] Sarkar, S. and Lakshmanan, B., (1991), *AIAA Journal*, 29(5), 748–749.

[8] Quirk, J., (1992), ICASE Report 92-64.

[9] Chalasani, S., Senguttuvan, V., Thompson, D., and Luke, E., (2008), *Communications in Numerical Methods in Engineering*, 24(6), 435–448.

[10] Engel, C. D., Praharaj, S. C., and Schmitz, C. P., (1998), REMTECH Report RTR 123-01.

[11] Schlicting, H., and Kersten, (2001), *Boundary Layer Theory*, 8th Ed.

[12] Miskovish, R. S., Shah, P., and Spottswood, S. M., (2010) 2010 SIMULIA Customer Conference.

[13] Spottswood, S. M. to Shah, P., (2009), email communication.

[14] Laganelli, A. L., and Wolfe. H. F., (1993), *Journal of Aircraft*, 30(6), 962–970.

[15] Librescu, L., Marzocca, P., Silva, W., (2002), Journal of Aircraft, 39(5), 802–812.

Appendix A: The properties of Inconel X-750 that were used in the above analysis are listed in Table 1 and are based on data found in MIL-HDBK-5J. The data in the figures below were linearly extrapolated in the temperature range of 1600 to 2000 °F. The stress-strain curves in Figure 27 assume linear stress-strain variation up to the yield stress data shown in Figure 28. The plastic portion of the curve was assumed to begin at the yield stress and continue to the ultimate stress (also shown in Figure 28). At the ultimate stress, the strain was assumed to be 0.2. The coefficient of thermal expansion (CTE), thermal conductivity, and specific heat are plotted as functions of temperature in Figure 29 and Figure 30.

Table 1. Inconel X-750 material properties

Density	0.298 lb/in^3
Poisson's Ratio	0.3

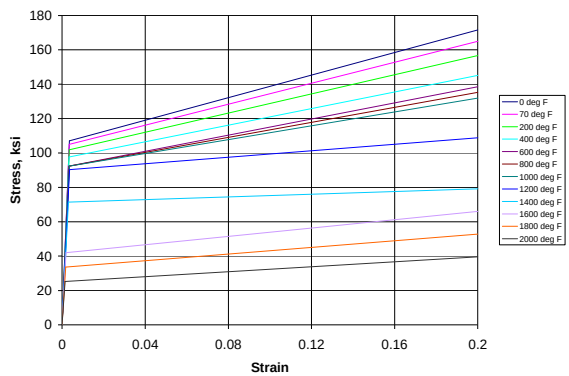

Figure 27. Stress-strain versus temperature for Inconel X-750

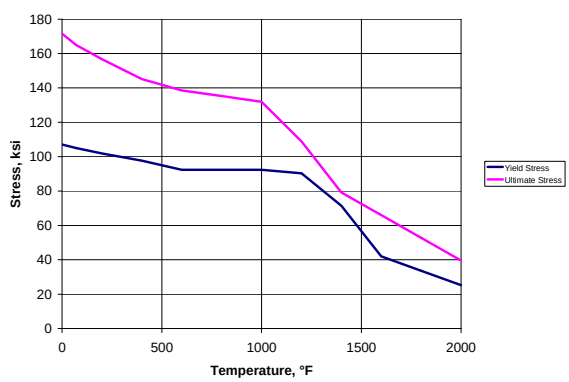

Figure 28. Yield and ultimate stress versus temperature for Inconel X-750

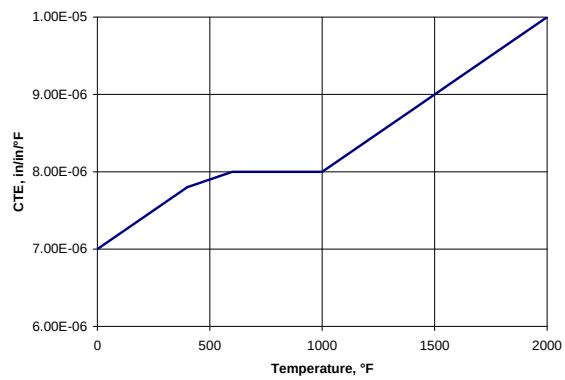

Figure 29. Coefficient of thermal expansion (CTE) versus temperature for Inconel X-750

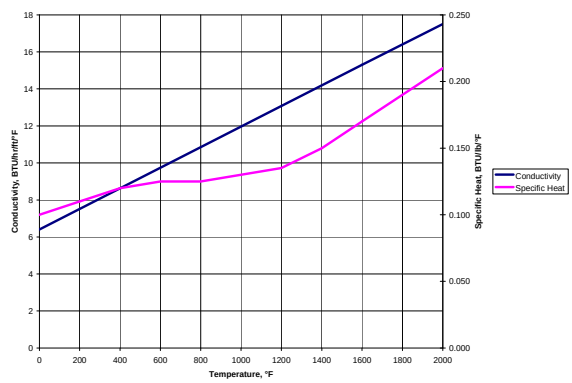

Figure 30. Thermal conductivity and specific heat versus temperature for Inconel X-750